J. Fluid Mech. (2013), *vol.* 721, *pp.* 199–224.
doi:10.1017/jfm.2013.73

Thermal boundary layer structure in turbulent Rayleigh–Bénard convection in a rectangular cell

Quan Zhou[1,2] **and Ke-Qing Xia**[2,†]

[1]Shanghai Institute of Applied Mathematics and Mechanics, Shanghai University, Shanghai 200072, China

[2]Department of Physics, The Chinese University of Hong Kong, Shatin, Hong Kong, China

(Received 3 October 2012; revised 24 January 2013; accepted 29 January 2013; first published online 13 March 2013)

We report high-spatial-resolution measurements of the thermal boundary layer (BL) properties in turbulent thermal convection. The experiment was made near the lower conducting plate of a water-filled rectangular convection cell of height 0.76 m, with a Prandtl number $Pr = 4.3$ and over the Rayleigh-number range $2 \times 10^{10} < Ra < 7 \times 10^{11}$. Time series of the local temperature at various vertical distance z from the plate were measured. Statistical properties of the profiles of the temperature, i.e. the mean temperature $\langle T \rangle$, fluctuating temperature root mean square (r.m.s.) σ_T, temperature skewness S_T, and flatness F_T, and those of the temperature time derivative, i.e. the r.m.s. σ'_T, skewness S'_T and flatness F'_T of the derivative, are studied. It is found that most of these quantities exhibit some degree of invariability with Ra, especially for the regime inside the thermal BL. When comparing with the mean temperature profiles, the profiles of the second moment of temperature seem to possess a higher level of universality. It is shown that the distance δ_σ from the plate to the maximal temperature r.m.s. position provides a natural length scale for the characterization of the thermal BL, as the statistical properties of the temperature field, such as its r.m.s., skewness and flatness, are all sharply different below and above this length scale, i.e. below δ_σ, σ_T increases linearly with the vertical distance z from the plate and S_T is close to zero and F_T is close to three and both quantities remains nearly constant, whereas above δ_σ the decay of σ_T obeys a logarithmic behaviour and S_T and F_T both exhibit a hill-like structure. It is also found that near the plate $\langle T \rangle$, σ_T and σ'_T all increase linearly with z. Our observations further reveal that such linear dependence occurs within a self-similar region of the thermal BL, where the temperature probability density functions can be scaled onto a single distribution that differs slightly from the Gaussian distribution. The Ra-dependencies of various thermal BL properties are also studied and our results yield $\delta_{th}/H = (6.85 \pm 0.70)Ra^{-0.33\pm0.03}$, $\delta_\sigma/H = (2.86 \pm 0.30)Ra^{-0.31\pm0.03}$ and $\delta'_\sigma/H = (25 \pm 3)Ra^{-0.38\pm0.05}$, where H is the height of the cell, δ_{th} and δ'_σ are the BL thicknesses determined respectively from the profiles of $\langle T \rangle$ and σ'_T.

Key words: Bénard convection, boundary layer structure, turbulent convection

† Email address for correspondence: kxia@phy.cuhk.edu.hk

1. Introduction

Turbulent Rayleigh–Bénard (RB) convection, i.e. an enclosed fluid layer heated from below and cooled from above, is a classical model system that has long been used to study the complicated convection phenomenon that occur ubiquitously in nature and in many engineering applications (Ahlers, Grossmann & Lohse 2009; Lohse & Xia 2010; Chillà & Schumacher 2012). The convective motion enhances dramatically the heat transport through the fluid layer, and understanding its nature is of fundamental interest and of great importance in the study of turbulent RB convection. The global heat transport is usually measured in terms of the Nusselt number Nu, defined as

$$Nu = \frac{J}{\chi \triangle / H}, \tag{1.1}$$

which depends on the turbulent intensity and the fluid properties that are characterized, respectively, by the Rayleigh number Ra and the Prandtl number Pr, namely

$$Ra = \frac{\alpha g \Delta H^3}{\nu\kappa} \quad \text{and} \quad Pr = \frac{\nu}{\kappa}, \tag{1.2}$$

where J is the heat-current density across the fluid layer with a height of H and with an applied temperature difference of Δ, g the gravitational acceleration, and α, ν, χ and κ are the thermal expansion coefficient, kinematic viscosity, thermal conductivity and thermal diffusivity of the convecting fluid, respectively.

The velocity and temperature fields within a very thin layer at the top and bottom plates, i.e. the kinematic and thermal boundary layers (BLs), play an essential role in the thermal convection system, especially in the global heat transport across the fluid layer. For example, the Nusselt number Nu is related, directly and intimately, to the thickness of the top and bottom thermal BLs because within which essentially all of the temperature drop of the system occurs and heat is transported mainly via conduction. In addition, almost all theories put forward to predict the relation between Nu and (Ra, Pr) are based on certain assumptions for the BLs, such as the stability assumption of the thermal BL for the early marginal stability theory (Malkus 1951), the laminar BL assumption for the Grossmann & Lohse (2000, 2001, 2004) theory and the turbulent BL assumption for the theories of Shraiman & Siggia (1990), of Dubrulle (2001, 2002), and of Grossmann & Lohse (2011) for the multiple scaling in the so-called ultimate regime. On the other hand, theories with different assumptions for the BL properties may yield the same predictions for the global quantities, such as the Nu–Ra scaling relation (Castaing *et al.* 1989; Shraiman & Siggia 1990). Therefore, direct characterization of the BL properties is of great importance for validating all of these assumptions and to gain an insight into the nature of turbulent heat transfer in turbulent RB system. However, compared with the large number of global heat transport measurements for various working fluids and cell geometries with wide parameter range and great precision (Castaing *et al.* 1989; Chavanne *et al.* 1997, 2001; Ashkenazi & Steinberg 1999; Glazier *et al.* 1999; Niemela *et al.* 2000; Ahlers & Xu 2001; Lam *et al.* 2002; Roche *et al.* 2002, 2010; Xia, Lam & Zhou 2002; Funfschilling *et al.* 2005; Sun *et al.* 2005; Niemela & Sreenivasan 2006; He *et al.* 2012; Zhou *et al.* 2012), experimental studies of the BL properties, especially the thermal BL structures in the high-Rayleigh-number regime, are rather limited. The objective of the present experimental investigation is to fill this gap by performing high-spatial-resolution measurements of temperature profiles in the vertical direction off the bottom plate in a water-filled rectangular cell of height 0.76 m and over the Rayleigh-number range $2 \times 10^{10} < Ra < 7 \times 10^{11}$.

Before the detailed presentation of our results, we first briefly review previous measurements of the thermal BL in turbulent RB system. Table 1 summarizes results of the temperature profiles and of scaling properties of the thermal BL thickness from some recent experimental studies.

1.1. *Scaling of the thermal BL thickness*

From an experimental point of view, the thermal BL thickness can be determined from either the time-averaged temperature profiles or the temperature root-mean-square (r.m.s.) profiles. For the former, the thickness δ_{th} is defined as the distance at which the tangent of the mean-temperature profile at the plate crosses the bulk temperature, while the later yields the thickness δ_σ that is the distance from the plate to the maximal temperature r.m.s. position. Tilgner *et al.* (1993) measured δ_{th} in a cubic cell filled with water at fixed Ra ($=1.1 \times 10^9$) and Pr ($=6.6$) and found in their case that the thermal BL is entirely buried in the viscous BL. Belmonte *et al.* (1993, 1994) further made thermal BL measurements in a cubic cell filled with room-temperature gas ($Pr = 0.7$) and over the Rayleigh number range from 5×10^5 to 10^{11} and their results showed that $\delta_{th} \simeq \delta_\sigma \sim Ra^{-2/7}$ for $Ra > 2 \times 10^7$. Naert *et al.* (1997) carried out measurements of the thermal BL thickness in mercury ($Pr = 0.024$) over the Rayleigh number range $10^6 < Ra < 10^8$, where the viscous BL is found to be thinner than the thermal one. Their results showed that δ_{th} coincides with δ_σ and both scale as $Ra^{-0.2\pm0.02}$. The spatial structures of the thermal BL in water and in the regime $10^8 < Ra < 10^{10}$ are systematically studied first by Lui and Xia in a cylindrical cell (Lui & Xia 1998) and then by Wang and Xia in a cubic cell (Wang & Xia 2003). Both of these works showed that the BL thickness above the bottom plate depends on the horizontal positions and the scaling exponent of δ_{th} with Ra varies between -0.35 and -0.28. However, this position dependence is suggested to eventually vanish, i.e. δ_{th} tends to become uniform across the plate, at very high Ra. This behaviour can now be understood from the shape evolution in the circulation path of the large-scale circulation (LSC). It was observed that the shape of the LSC evolutes from a tilted and nearly elliptical shape at low Ra to a squarish shape at high Ra (Niemela & Sreenivasan 2003; Xia, Sun & Zhou 2003; Sun & Xia 2005). The squarish-shaped LSC at high Ra would make the mean flow near the horizontal plates parallel to the plates and hence lead to the uniformity of the BLs that are modulated and stabilized by the shear of the mean flow. Recent experiments using air as working fluid in a cylindrical cell over the Ra range $10^9 < Ra < 10^{12}$ by du Puits *et al.* (2007*b*) reported that $\delta_{th} \sim Ra^{-0.2540}$ and $\delta_\sigma \sim Ra^{-0.4051}$. Maystrenko *et al.* (2007) extended these measurements to the range $6 \times 10^7 \leqslant Ra \lesssim 6 \times 10^8$ in a long rectangular cell, but still using air as a working fluid, and they found that $\delta_\sigma \sim Ra^{-0.43}$ above the middle of a convection roll structure. In a more recent experimental work, Sun *et al.* (2008) studied systematically the properties of both the viscous and thermal BLs in a rectangular cell with Ra varying from 10^9 to 10^{10} and the results showed that $\delta_{th}/H = 6.10Ra^{-0.32\pm0.05}$.

1.2. *Profiles of the mean temperature and temperature r.m.s.*

How the mean temperature $\langle T \rangle$ and temperature r.m.s. $\sigma_T = \langle (T - \langle T \rangle)^2 \rangle^{1/2}$ change with the vertical distance z from the plate, especially for the regions within the thermal BL and inside the mixing zone, is also an issue of considerable interest in the study of turbulent thermal convection, partly due to its relevance to the heat transport from the plates and to the differentiating of various models that made different predictions for the distribution of the temperature profiles, such as power-law profiles predicted

https://doi.org/10.1017/jfm.2013.73 Published online by Cambridge University Press

Sources	Geometry	Fluid	Ra	Pr	γ_{th}	γ_σ	$\langle T\rangle(z)$	$\sigma_T(z)$
(*a*,*b*,*c*)	Cubic	Water	1.1×10^9	6.6	—	—	$\sim z$	$\sim z^{-0.8}$ or $\ln(z)$
(*a*,*b*,*c*)	Cubic	SF_6	$5\times10^5\sim10^{11}$	0.7	-0.29 ± 0.01	—	$\sim z$	$\sim z^{-0.72}$ or $\ln(z)$
(*d*)	Rectangular	Water	$10^6\sim4\times10^8$	4	—	—	—	$\ln(z)$
(*e*)	Cylindrical	Mercury	$10^6\sim10^8$	0.024	-0.2 ± 0.02	-0.2 ± 0.02	—	—
(*f*)	Cylindrical	Water	$10^8\sim10^{10}$	7	$-0.35\sim-0.28$	—	$\sim z$	—
(*g*)	Rectangular	Water	$10^7\sim10^9$	$4.0\sim6.7$	—	—	—	$\sim\ln(z)$
(*h*)	Cubic	Water	$10^8\sim10^{10}$	7	-0.28	—	$\sim z$	—
(*i*)	Cylindrical	Air	$10^9\sim10^{12}$	0.7	-0.25	-0.41	$\sim z^{0.47\sim0.76}$	$\sim z^{-0.42\sim-0.30}$
(*j*)	Rectangular	Air	$6\times10^7\sim6\times10^8$	0.7	—	-0.43	$\sim z^{0.51\sim0.68}$	$\sim z^{-0.77\sim-0.43}$ or $\ln(z)$
(*k*)	Rectangular	Water	$10^9\sim10^{10}$	4.3	-0.33 ± 0.05	—	$\sim z$	$\sim z^{-0.77\sim-0.6}$ or $\ln(z)$
(*l*)	Cylindrical	SF_6	$4\times10^{12}\sim10^{15}$	0.8	—	—	$\sim\ln(z)$	$\sim\ln(z)$
(*m*)	Cylindrical	Air	$3.4\times10^9\sim10^{12}$	0.7	-0.24	—	—	—
Present	Rectangular	Water	$2\times10^{10}\sim7\times10^{11}$	4.3	-0.33 ± 0.03	-0.31 ± 0.03	$\sim z$	$\sim\ln(z)$

TABLE 1. Summary of experimental studies of the thermal BL properties: scaling exponents γ_{th} and γ_σ of δ_{th} and δ_σ with Ra, respectively, the shape of the $\langle T\rangle$ profiles within the thermal BL and that of the σ_T profiles inside the mixing zone. A dash indicates that an analysis was not performed or such data were not discussed in the paper. The sources are: (*a*) Tilgner, Belmonte & Libchaber (1993); (*b*) Belmonte, Tilgner & Libchaber (1993); (*c*) Belmonte, Tilgner & Libchaber (1994); (*d*) Chillá *et al.* (1993); (*e*) Naert, Segawa & Sano (1997) (*f*) Lui & Xia (1998); (*g*) Fernandes & Adrian (2002); (*h*) Wang & Xia (2003); (*i*) du Puits *et al.* (2007*b*); (*j*) Maystrenko, Resagk & Thess (2007); (*k*) Sun, Cheung & Xia (2008); (*l*) Ahlers *et al.* (2012); (*m*) Li *et al.* (2012).

by Prandtl (1932) for $\langle T \rangle$ and by Priestley (1959) and Adrian (1996) for σ_T, and logarithmic profiles by Castaing *et al.* (1989) for σ_T. Here $\langle \cdots \rangle$ represents a time average. Experimental studies, however, have shown some ambiguous observations.

For the mean-temperature profile, early measurements revealed that $\langle T \rangle$ increases linearly with z from the plate and the linear region covers, on average, nearly 60 % of the thickness of the thermal BL (Belmonte *et al.* 1994). Some later experiments further revealed that the $\langle T \rangle$ profile can be divided into three regions: a linear region near the plate where heat is transported upwards mainly by conduction; a 'horizontal' or plateau region away from the plate where the gradient of the mean temperature is nearly zero and convection dominates; and a transitional region in between (Lui & Xia 1998; Wang & Xia 2003). These studies also focused on the universality of the mean-temperature profiles and showed that the scaled profiles at various positions but for the same *Ra* are self-similar, whereas those measured at different *Ra* do not show an invariant form (Lui & Xia 1998; Wang & Xia 2003). In a theoretical study, Ching (1997) found a connection between the shape of the temperature profile and the heat flux. Shishkina & Thess (2009) found that near the heating and cooling plates the non-dimensional temperature profiles obey neither a logarithmic nor a power law, but can be approximated by a universal stretched exponential function.

For the temperature r.m.s. profile, a well-defined maximum $(\sigma_T)_{max}$ was found for the profile (Tilgner *et al.* 1993; Belmonte *et al.* 1993, 1994) and the distance from the position of this maximal temperature fluctuation to the plate was suggested to be a measure of the thermal BL thickness (Tilgner *et al.* 1993). Wang & Xia (2003) further found that the temperature r.m.s. profiles measured at the same position but different *Ra* can be brought to collapse onto a single curve, whereas those with different positions but for the same *Ra* do not show a universal form. For the shape of the temperature r.m.s. profile within the regime of the so-called mixing zone, Chillá *et al.* (1993) found a logarithmic dependence of σ_T on z and related this dependence to the exponential tails of the spatial distribution of temperature fluctuations. Fernandes & Adrian (2002) also reported the observed logarithmic profile for σ_T. In contrast, du Puits *et al.* (2007*b*) observed that the profiles of σ_T obey a power-law behaviour with the scaling exponents depending on both *Ra* and Γ. In our previous work, we have made a systematically experimental study of the viscous BL properties (Sun *et al.* 2008). Profiles of the mean temperature and its fluctuations in the Rayleigh-number range $10^9 < Ra < 2 \times 10^{10}$ near the plate were also measured and, hence, the thermal BL. Our results, however, showed that both the power law and the logarithmic dependence can be used to fit the measured σ_T profiles to some degree, which may be due to the moderate *Ra* in this study. Note that similar results have also been observed previously (Belmonte *et al.* 1994; Maystrenko *et al.* 2007).

Very recently, Ahlers *et al.* (2012) studied the interior of turbulent RB convection over a high-*Ra* range by using a combination of experiment ($4 \times 10^{12} \leqslant Ra \leqslant 10^{15}$) and simulation ($Ra = 2 \times 10^{12}$). They found that both the mean and r.m.s. temperatures vary logarithmically with the distance from the plates over a wide range of z/H. These authors also showed that the amplitude of the logarithmic profile is largest near the cell's sidewall and becomes small when the cell's centre is approached.

The apparent disagreements of the above results indicate that experimentally how $\langle T \rangle$ and σ_T vary with z is far from settled, which prompted us to carry out the present experiment. Here, we report new measurements of the thermal BL properties, made in a rectangular cell with height 0.76 m, performed with high spatial resolution, and extended to a higher *Ra* range $2 \times 10^{10} < Ra < 7 \times 10^{11}$. Our results reveal that $\langle T \rangle$

and σ_T both increase linearly with z for $z \lesssim \delta_\sigma$ (within the thermal BL), while the profiles of σ_T follows a logarithmic behaviour inside the mixing zone.

1.3. *Profiles of skewness of temperature derivative (increments)*

Belmonte & Libchaber (1996) used the skewness of the temperature time derivative to study the coherent structures of thermal fluctuations in a cubic cell filled with pressured gas (helium, nitrogen and sulfur hexafluoride) at room temperature and spanned a range of Ra from 5×10^5 to 10^{11} with $Pr = 0.7$. Their results showed that near but outside the cold thermal BL the skewnesses of both the temperature and its time derivative are smaller than zero, corresponding to the sharp front of thermal plumes and indicating the active signature of the temperature fluctuations. Zhou & Xia (2002) studied the profiles of the skewnesses of the 'plus' and 'minus' temperature increments in a water-filled cylindrical cell at fixed Prandtl number $Pr \simeq 4$ and over varying Rayleigh numbers $2 \times 10^8 < Ra < 2 \times 10^{10}$. They found that a gap exists between the two skewnesses within the region where most of plume mixing, merging and clustering take place (called the mixing zone), but vanishes inside the thermal BL and inside the convective central core. However, the detailed information of the temperature derivative or increments profiles are still missing, which is one of the objectives of the present study.

1.4. *Organization of the present paper*

The remainder of this paper is organized as follows. In § 2, we describe the convection cell used in the experiments and details of high-spatial-resolution measurements of the local temperature. The experimental results are presented and analysed in § 3, which is divided into five parts. Section 3.1 compares and discusses the time series of temperature measured at different vertical distances from the bottom plate. We present and discuss the statical properties of the temperature profiles in § 3.2 and of the temperature time derivative profiles in § 3.4 and show the analysis of the self-similar regime in § 3.3. The Ra dependence of the thermal BL properties are presented and discussed in § 3.5. We summarize our findings and conclude in § 4.

2. Experimental set-up and parameters

The purpose of the investigation is to study the thermal BL structure, which can be used to differentiate the various theoretical models that have different assumptions for the BL. Since most of these models are essentially two-dimensional and the BL properties in convection cells with some kind of axial symmetry, such as the most widely used cylindrical cell, will be inevitably modified and perturbed by the stochastic azimuthal meandering (Brown & Ahlers 2006; Xi, Zhou & Xia 2006) and the sloshing motion (Xi *et al.* 2009; Zhou *et al.* 2009) of the LSC, we chose a rectangular-shaped cell to perform the measurements of the temperature profiles and the thermal BL thickness. A detailed description of the apparatus has been discussed previously (Xia *et al.* 2003). The experiment was conducted at the Chinese University of Hong Kong. The length L, width W and height H of the cell are 81 cm × 20 cm × 76 cm, respectively, and the cell aspect ratios are thus given by $\Gamma_x \equiv L/H = 1.07$ and $\Gamma_y \equiv W/H = 0.26$. With this geometry, the axis symmetry does not exist and the LSC would be confined in the (x, z) plane (Xia *et al.* 2003; Zhou, Sun & Xia 2007*b*; Zhou & Xia 2008) (see figure 1). Therefore, the perturbation of the stochastic azimuthal meandering and the sloshing motion of the LSC to the thermal BL can be neglected and the velocity in this plane will be the dominant component of the LSC (Xia *et al.* 2003).

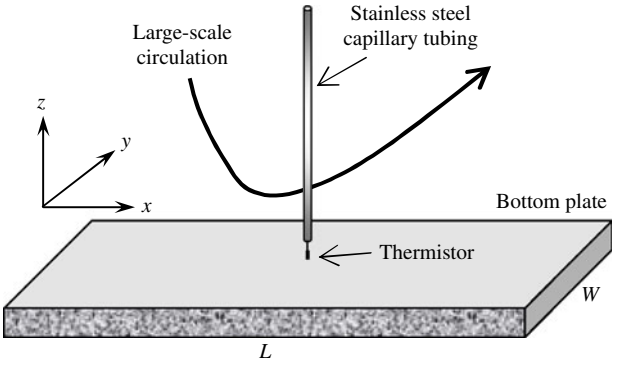

FIGURE 1. Schematic drawing of the temperature measurement system above the bottom plate and the coordinates for the experiment.

The temperature profiles presented here were measured along the vertical axis that passes through the centre of the bottom plate and the measurement coordinate system is defined in figure 1. A glass-encapsulated thermistor (AB6E3-B10KA103J, Thermometrics) that has a sensing head of 0.24 mm in diameter and a thermal time constant of 10 ms in water, is used to measure the local temperature field above the bottom plate. Therefore, the smallest distance that can be reached between the temperature probe and the bottom plate is 0.12 mm, corresponding to one half the sensor's diameter. The thermistor is threaded through a stainless steel capillary tubing with outer diameter of 2 mm and inner diameter of 1 mm and then fixed on a computer-controlled transitional stage that can be moved in steps of 0.001 mm along the vertical direction. This arrangement allows the precise adjustment of the vertical distance between the sensor and the bottom plate. The accuracy of the thermistor is determined mainly by the calibration process and was better than 0.01 °C in the present case.

Distilled and degassed water was used as the working fluid. During the measurements, the mean temperature of the working fluid was kept at 40 °C, corresponding to the Prandtl number $Pr = 4.3$. The cell was levelled to within $0 \pm 0.06°$ in all measurements. By changing the temperature difference Δ between the top and bottom plates, Ra was varied from 2.6×10^{10} to 6.4×10^{11} while Pr was kept nearly constant. To avoid the heat leakage, the flanges of the top and bottom plates were insulated by 3 cm thick nitrile rubber sheets and the system was wrapped by several layers of Styrofoam. For each Ra, at least 55 vertical positions below $z = 50$ mm (z is the distance from the bottom plate) were chosen to perform the measurements and at each position the resistance of the thermistor was recorded by a 6.5-digit multimeter (Keithley Model 2700) with a sampling rate $\sim$15 Hz and over a time span of 40–100 min depending on Ra. The temperature profiles were then obtained from the measured resistance using a calibration conversion curve. To extend the temperature profiles to the central core region of the convection cell, we also measured the local temperature field at an additional five vertical positions between $z = 50$ mm and $z = H/2 = 380$ mm for $Ra = 4.0 \times 10^{10}$ and 3.2×10^{11}. For the data reproducibility, we have performed two sets of independent measurements for $Ra = 9.8 \times 10^{10}$. Within the experimental uncertainty, the two measured data show the same results for the temperature profiles up to the fourth moment.

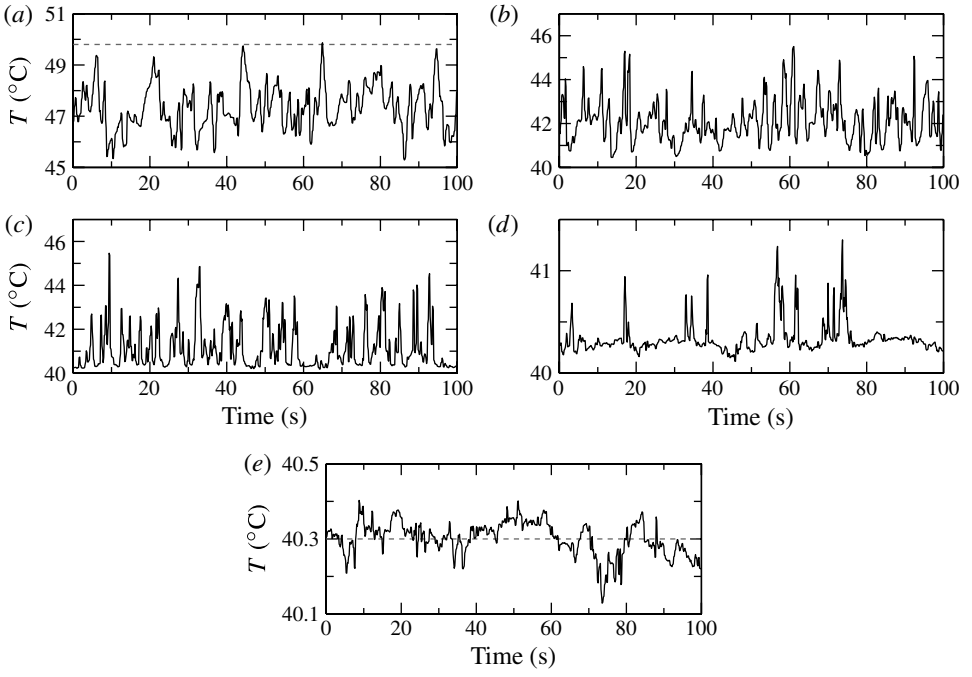

FIGURE 2. Time series of temperature T measured at $Ra = 3.2 \times 10^{11}$ and at different z from the bottom plate. The dashed lines in (*a*,*e*) mark the measured mean temperatures of the bottom plate and the bulk fluids, respectively: (*a*) $z = 0.20$ mm $(0.28\delta_{th})$; (*b*) $z = 0.71$ mm $(0.99\delta_{th})$; (*c*) $z = 2.33$ mm $(0.99\delta_u)$; (*d*) $z = 28.3$ mm (mixing zone); (*e*) $z = 380$ mm (cell centre).

3. Results and discussion

3.1. *Time series of the local temperature*

Figure 2 shows the time series, over a time interval of 100 s, of the local temperature measured at five different distances from the bottom plate. The corresponding temperature probability density functions (p.d.f.) are plotted in figure 3. The measurements were carried out at $Ra = 3.2 \times 10^{11}$. At this Ra, the bottom plate temperature T_b and the mean bulk temperature T_0 measured at cell centre are, respectively, 49.8 and 40.3 °C, the thickness of the thermal BL $\delta_{th} = 0.72$ mm and that of the viscous BL is $\delta_u = 2.36$ mm (Zhou & Xia 2010). Therefore, the results shown in figures 2 and 3 correspond to several typical positions: (*a*) within the thermal BL; (*b*) at the edge of the thermal BL; (*c*) at the edge of the viscous BL; (*d*) far away from both the BLs and within the mixing zone; and (*e*) at the cell centre.

Figure 2(*a*) shows the local temperature at the position ($z = 0.20$ mm) that is very close to the bottom plate and inside the thermal BL. The measured temperature fluctuates around its mean value that is close to the bottom plate temperature T_b (indicated by the dashed line in figure 2*a*). The corresponding p.d.f. (diamonds, shown in green online) shown in figure 3(*a*) revealed that the distribution of the temperature at such position has a nearly Gaussian shape, although a little asymmetry can be found from its two tails, i.e. the temperature is skewed slightly toward higher temperature values. As we shall see in § 3.3, this distribution is typical for the temperature within the thermal BL.

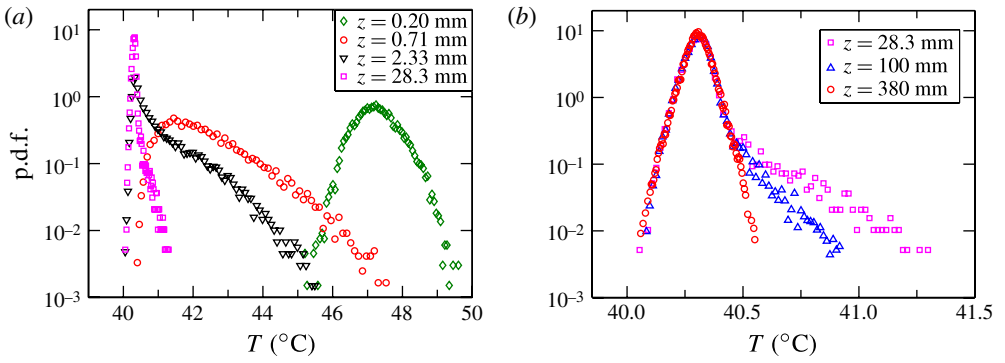

FIGURE 3. (Colour online) The p.d.f.s of the local temperature T measured at $Ra = 3.2 \times 10^{11}$ and at different z from the bottom plate.

When z is increased toward δ_{th}, the measured mean temperature decreases rapidly from close to T_b to the mean bulk temperature T_0 but its fluctuations increase. At $z = \delta_\sigma = 0.48$ mm the temperature r.m.s. reaches its maximal value. Figure 2(*b*) shows the measured temperature around the position of the thermal BL ($z = 0.71$ mm). One sees clearly that there are a large number of temperature bursts toward the high temperature values. These temperature bursts are manifestations of thermal plumes because the signal with a pulse-like shape, i.e. a temperature burst, would be detected when a thermal plume passing through the thermal sensor. Note that when expanding the time series, one can see the cliff-ramp-like structures as reported by Zhou & Xia (2002) and Xi *et al.* (2009), which are signatures of thermal plumes.

As the measuring position is further shifted far away from the thermal BL, the temperature time series, such as those shown in figure 2(*c*,*d*), seem to consist of contributions from two kinds of fluids: a fraction of tepid fluid that has a relatively constant background temperature and a fraction of very hot fluids that come from the bottom thermal BL and manifested as temperature bursts, i.e. the moving hot plumes. A remarkable feature revealed by these figures is that the fraction of hot fluids decreases at increasing distance from the thermal BL (figure 2*c*,*d*) and no such burst can be found at the cell centre (figure 2*e*), implying the decreasing plume number at increasing z. Further analysis indicates that the decrease of the number of temperature bursts occurs within the mixing zone, which is determined from the properties of the 'plus' and 'minus' temperature skewness profiles (Zhou & Xia 2002). As most plume mixing, merging, and clustering take place within the mixing zone (Castaing *et al.* 1989; Zhou, Sun & Xia 2007*a*), the plume number decreases within such a regime when away from the thermal BL (Zhou *et al.* 2007*a*). The decrease of the plume number can also be reflected by the evolution of the temperature p.d.f.s in figure 3(*b*). It is seen that as z increases the probability of observing higher temperature events (the right tail), corresponding to the number of thermal plumes (or temperature bursts), decreases and eventually vanishes near the cell centre. Meanwhile, the distribution of the bulk background temperature remains nearly unchanged and is similar to that of the central bulk region.

3.2. *Properties of the temperature profiles*

We discuss the temperature profiles in this section. As reported in § 1.2, contradicting observations exist regarding the time-averaged temperature profiles within the thermal

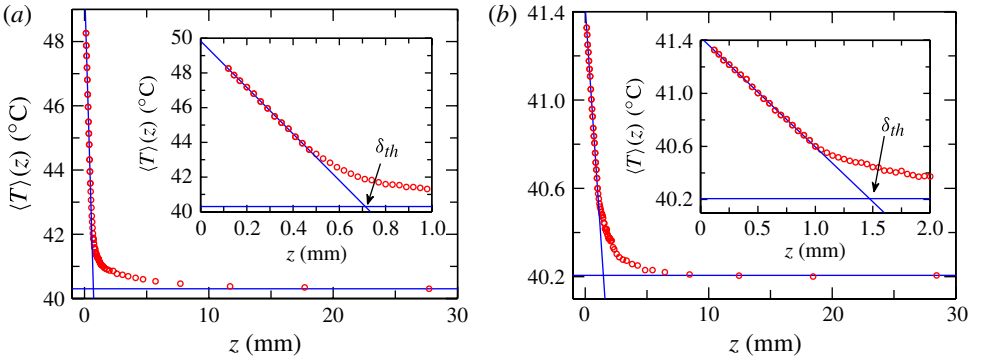

FIGURE 4. (Colour online) Profiles of the mean temperature $\langle T\rangle$ measured at $Ra = 3.2 \times 10^{11}$ (*a*) and 4×10^{10} (*b*). The insets show an enlarged portion of the profiles close to the plate. The solid lines illustrate the definition of the thermal BL thickness δ_{th}.

BL. Belmonte *et al.* (1994) observed a linear portion in the mean-temperature profiles, whereas du Puits *et al.* (2007*b*) observed that outside a very short linear regime near the plate the mean-temperature profiles obey a power-law behaviour. For reference, table 1 summarizes several recent experimental observations of the distribution of the mean-temperature profiles.

Figure 4 shows the results from typical profile measurements at $Ra = 3.2 \times 10^{11}$ and 4×10^{10}, where the mean temperature $\langle T\rangle$ is plotted as a function of the vertical distance z from the bottom plate (measurements were made up to $z = 50$ mm; as $\langle T\rangle$ remains constant after $z \gtrsim 20$ mm, for clarity, only data for z up to 30 mm are shown). It can be seen that when moving away from the bottom plate $\langle T\rangle$ first decreases dramatically in a very thin layer, then experiences a transition and finally tends to the mean bulk temperature. This agrees well with previous observations of three regions of the thermal BL (Lui & Xia 1998; Wang & Xia 2003). To see clearly the decreasing tendency of $\langle T\rangle$, we plot in the insets of figure 4 enlarged near-boundary portions of the $\langle T\rangle$ profiles. It is seen clearly from the figures that near the bottom plate the z dependence of $\langle T\rangle$ is linear. This linear region is found to hold for all Ra investigated, to cover nearly 60–70 % of δ_{th} and to be covered by 10–20 data points (depending on Ra). Further analysis of $\langle T\rangle$ indicates that within experimental uncertainty the extrapolation of the linear part of the temperature profile meets the temperature of the bottom plate T_b as z tends to zero. This is in agreement with some previous temperature measurements in room-temperature gases (Tilgner *et al.* 1993; Belmonte *et al.* 1993, 1994) and in water (Lui & Xia 1998; Wang & Xia 2003; Sun *et al.* 2008). Figure 4 also shows the definition of δ_{th} (as illustrated by solid lines). The Ra dependence of the thermal BL properties will be discussed in § 3.5.

In the present study, high-spatial-resolution temperature measurements allow us to examine systematically the universal properties of the mean-temperature profile near the thermal BL. To do this, we plot in figure 5(*a*) near-plate portions of five typical scaled profiles with their values of Ra indicated on the graph. Here $\Theta(z) \equiv [T_b - \langle T\rangle(z)]/(T_b - T_0)$ is the mean temperature (subtracted from that of the bottom plate) normalized by the temperature difference between the bottom plate and the bulk fluids, and the vertical distance z is scaled by the respective thermal BL thickness δ_{th}. We found that all profiles within the linear region show a universal form, whereas those within the transitional region cannot be simply scaled to collapse onto a

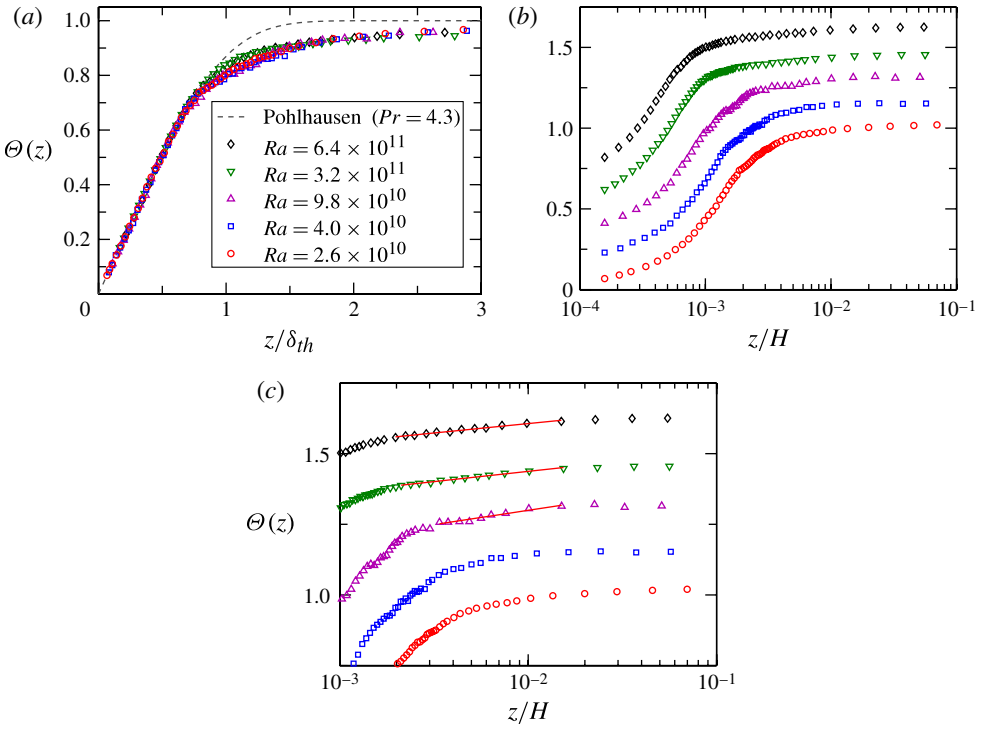

FIGURE 5. (Colour online) The scaled time-averaged temperature $\Theta(z) \equiv [T_b - \langle T \rangle(z)]/(T_b - T_0)$ as a function of the vertical position z in linear (*a*) and semi-log (*b*,*c*) plots for various Ra. The dashed line in (*a*) represents the temperature profile of a laminar, zero-pressure gradient BL according to Pohlhausen for $Pr = 4.3$. The solid lines in (*c*) are the logarithmic fits to the corresponding data. For clarity, the data in (*b*,*c*) have been shifted vertically.

single curve. The spread (non-universality) is due to BL fluctuations/plume emissions. Note that this feature was also observed by previous studies in both cylindrical (Lui & Xia 1998) and cubic (Wang & Xia 2003) cells.

For comparison, the theoretical temperature profile of a laminar, zero-pressure gradient BL, according to Pohlhausen (1921), is also plotted as a dashed line in figure 5(*a*). Within the transitional region of the profiles, one sees that the approach to asymptotic value is always slower than that of the laminar profile, which is similar to the velocity BL case (du Puits, Resagk & Thess 2007*a*; Sun *et al.* 2008). This can be attributed to the emissions of thermal plumes from the BLs. According to previous numerical studies (Zhou *et al.* 2010, 2011*b*; Scheel, Kim & White 2012; Stevens *et al.* 2012; Shi, Emran & Schumacher 2012; Verzicco 2012), the temperature profiles are much closer to the Pohlhausen profile, if they are resampled in the dynamical reference frame that fluctuates with the instantaneous thermal BL thickness. Owning to the nature of the measurement technique used in the present study, we are not able to obtain the instantaneous temperature profiles and thus cannot apply the dynamical BL rescaling analysis.

In figure 5(*b*), the scaled time-averaged temperature is also plotted as a function of z/H in a semi-log plot to see whether there is a logarithmic layer for the measured temperature profiles. There seems to exist a logarithmic range for the scaled temperature over roughly $2 \times 10^{-3} \lesssim z/H \lesssim 2 \times 10^{-2}$ for high-Ra cases. To

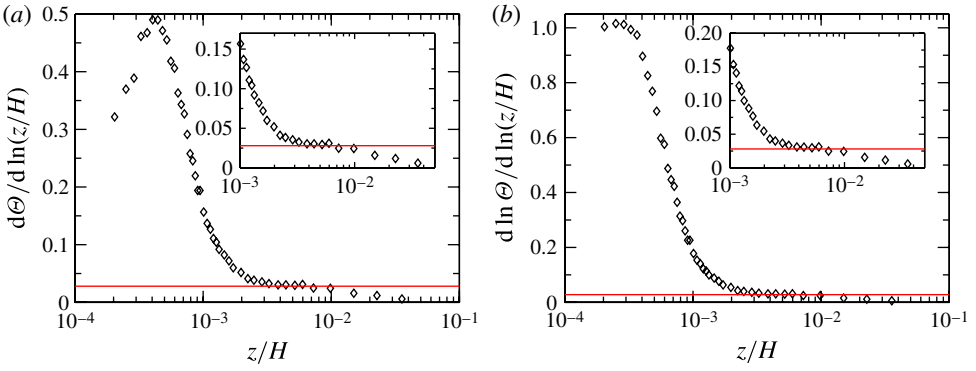

FIGURE 6. (Colour online) Diagnostic functions (*a*) $\mathrm{d}\Theta/\mathrm{d}\ln(z/H)$ (for logarithmic profile) and (*b*) $\mathrm{d}\ln\Theta/\mathrm{d}\ln(z/H)$ (for power-law profile) for $Ra = 6.4 \times 10^{11}$. The insets show an enlarged portion of the approximated plateau regions, respectively.

see this more clearly, we plot in figure 5(*c*) an enlargement of the relevant range. While one sees no discernible logarithmic ranges for the two low-Ra data sets, the three higher-Ra data sets seem to exhibit a logarithmic range as shown by respective solid lines in the figure. For the measured temperature profiles, we note that the logarithmic layer could be identified only for $Ra \geqslant 9.8 \times 10^{10}$ and the logarithmic range appears to be a little wider for higher Ra. Furthermore, if we adopt the definition $\Theta'(z) \equiv [\langle T\rangle(z) - T_0]/\Delta$ and use the logarithmic relation $\Theta'(z) = A \times \ln(z/H) + B$ to fit the relevant data, these yield $A = -0.022, -0.015, -0.014$ and $B = -0.101, -0.052, -0.040$ for $Ra = 9.8 \times 10^{10}, 3.2 \times 10^{11}, 6.4 \times 10^{11}$, respectively. We note that these fitted parameters are of the same order as those obtained recently by Ahlers *et al.* (2012). Nevertheless, the amplitude A of the logarithmic profiles are quite small and for the limited logarithmic range of less than one decade one can also use other functions to fit the data, such as a power-law function. To see this more clearly, we follow the idea of Shishkina & Thess (2009) and evaluate the diagnostic functions $\mathrm{d}\Theta/\mathrm{d}\ln(z/H)$ and $\mathrm{d}\ln\Theta/\mathrm{d}\ln(z/H)$. The diagnostic functions for logarithmic and power-law behaviours are plotted in figure 6(*a*,*b*), respectively, for $Ra = 6.4 \times 10^{11}$. A certain plateau might be seen from both functions within the range $3 \times 10^{-3} \lesssim z/H \lesssim 10^{-2}$, but one cannot tell which behaviour is better to describe the mean temperature profile in the bulk. Therefore, based on the present data we cannot state conclusively that there is a logarithmic layer for the temperature profiles along the cell's central line, and this will be the subject of future studies.

We now examine the r.m.s. temperature profiles. Figure 7(*a–d*) show the results for the profiles of the normalized temperature r.m.s. $\sigma_T/(\sigma_T)_{max}$ obtained at five typical Ra. The global features of the profiles shown in figure 7(*a*) are similar to previous measurements, i.e. $\sigma_T/(\sigma_T)_{max}$ first experiences a sharp increase near the plate, reaches its maximum at $z = \delta_\sigma$, and then decreases when the measuring position is shifted to the convective central core. We further found that $(\sigma_T)_{max}$ occurs at the position that is just located at the upper end of the linear portion of the $\langle T\rangle$ profile and the ratio $\delta_\sigma/\delta_{th}$ varies between 0.6 and 0.7 and is essentially independent of Ra. This value is a little smaller than those found by Belmonte *et al.* (1994) in a cubic cell filled with SF_6 ($\delta_\sigma/\delta_{th} \simeq 1$) and by Wang & Xia (2003) in a cubic cell filled with water ($\delta_\sigma/\delta_{th} = 0.8$). A possible explanation for this difference could be due to the different large-scale flow modes that is induced by different geometries of the convection cells. Figure 7(*a*) also

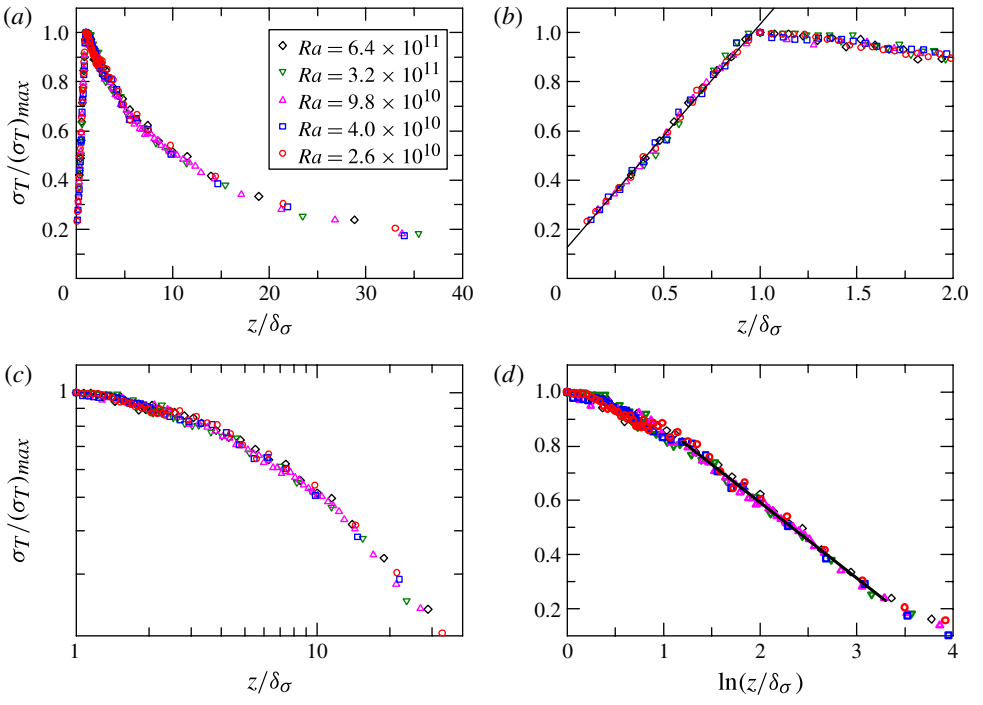

FIGURE 7. (Colour online) Profiles of the normalized temperature r.m.s. $\sigma_T/(\sigma_T)_{max}$ versus the normalized vertical distance z/δ_σ from the bottom plate in linear–linear (*a*,*b*), log–log (*c*) and semi-log (*d*) plots at various *Ra*. The solid lines in (*b*,*d*) are, respectively, the linear and the logarithmic fits to the corresponding portions of the profiles.

shows that the normalized profiles measured at different *Ra* can be brought to collapse onto a single curve, which is in contrast with the profiles of the mean temperature that exhibit certain spread within the transitional region. This may be understood by the fact that we use the right normalization factor, i.e. $(\sigma_T)_{max}$, to normalize the r.m.s. temperature profile, as $(\sigma_T)_{max}$ is a measure of the degree of fluctuations for the corresponding *Ra*. This also suggests that the 'fluctuating quantities' are more universal than the mean quantities in turbulent thermal convection. This feature agrees well with the results obtained in a cubic cell (Wang & Xia 2003).

When looking more carefully at the profiles plotted in different scales, two other remarkable features are worthy to note. The first is the increase of the temperature fluctuations σ_T within the thermal BL. As shown in figure 7(*b*), the z dependence of $\sigma_T/(\sigma_T)_{max}$ is linear before σ_T reaches its maximum. The solid line in figure 7(*b*) is the linear fit to the profiles for $z \lesssim \delta_\sigma$. Together with the results for the $\langle T \rangle$ profiles, we conclude that near the plate both the mean and r.m.s. values of the temperature increase *linearly* with z. It can also be seen from figure 7(*b*) that the vertical-axis intercept of the fitting line is non-zero. The non-zero value of σ_T as $z \to 0$, although not large but nonetheless beyond our experimental uncertainty, reflects the non-zero temperature fluctuations in the plate.

The second feature is about the decay of the temperature fluctuations σ_T inside the mixing zone. Figure 7(*c*,*d*) plot the same data of the normalized temperature r.m.s. $\sigma_T/(\sigma_T)_{max}$ versus the normalized vertical distance z/δ_σ from the bottom plate

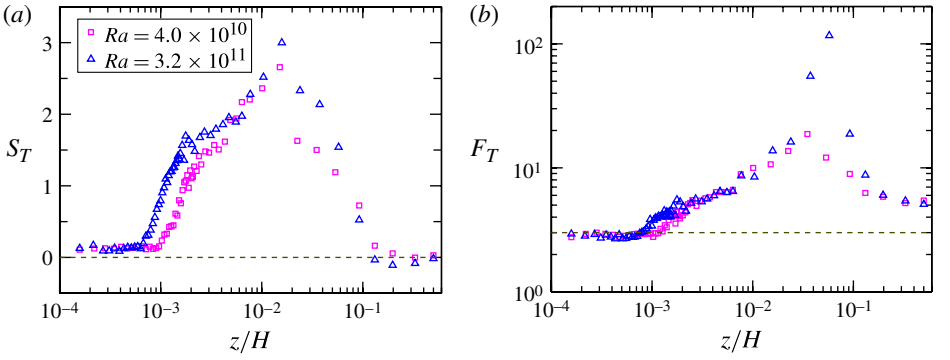

FIGURE 8. (Colour online) Profiles of the skewness S_T (a) and the flatness F_T (b) of temperature. Here the vertical distance z has been normalized by the cell height H.

for $z \geqslant \delta_\sigma$ on log–log and semi-log scales, respectively. The solid line in figure 7(d) is the best logarithmic fit to the corresponding portion of the profiles. One sees that no discernible scaling range can be identified from the log–log plot (figure 7c), while a logarithmic function $\sigma_T \sim \ln z$ is observed to provide the best description of the data within the fitting region $1.2 \lesssim \ln(z/\delta_\sigma) \lesssim 3.2$ when they are plotted on semi-log scale (figure 7d). Hence, our experiment supports the logarithmic variation of the r.m.s. temperature profile, at least for the present parameter ranges. To compare with previous measurements, we also plotted (not shown here), on a semi-log scale, σ_T, normalized by the temperature difference $\triangle$ across the cell, as a function of z/H. The slope α' for the logarithmic profile obtained from that plot is found to change from -0.024 to -0.015, which is comparable with those found by Sun *et al.* (2008) in a relatively low Ra range ($-0.025 \lesssim \alpha' \lesssim -0.017$).

We would like to stress that σ_T experiences a sharp transition at $z = \delta_\sigma$, which suggests that δ_σ is a natural scale to describe (small-scale) properties associated with plumes. Therefore, in the remainder of this paper, we use δ_σ, rather than δ_{th}, to normalize the vertical distance z from the bottom plate.

Continuing to the profiles of the high-order moments of temperature. The skewness, the third-order moment, is a global measure of the asymmetry of the sampled-data (such as temperature in the present case) distribution around its mean value and the flatness, the fourth-order moment, characteristically describes whether the sampled-data distribution is peaked or flat relative to a Gaussian distribution. Here, the skewness and the flatness of temperature are given, respectively, by

$$S_T = \langle (T - \langle T \rangle)^3 \rangle / \sigma_T^3 \quad \text{and} \quad F_T = \langle (T - \langle T \rangle)^4 \rangle / \sigma_T^4. \tag{3.1}$$

By definition, the skewness of a symmetric distributed quantity is zero and the flatness of a Gaussian-distributed quantity is three. Figure 8(a,b) show, respectively, the skewness S_T and the flatness F_T of temperature versus the vertical distance z. Here z has been normalized by the cell height H and our profiles cover half height of the convection cell, i.e. from the bottom plate to the cell centre. The figure reveals three distinct regions for both S_T and F_T in the convection cell. First is the region inside the thermal BL, in which both S_T and F_T change very little with position. The value of S_T is small and positive and that of F_T is slightly smaller than three, which confirm quantitatively the fact, observed from the time series and the p.d.f.s of temperature in § 3.1, that within the thermal BL the temperature is nearly Gaussian distributed, but a

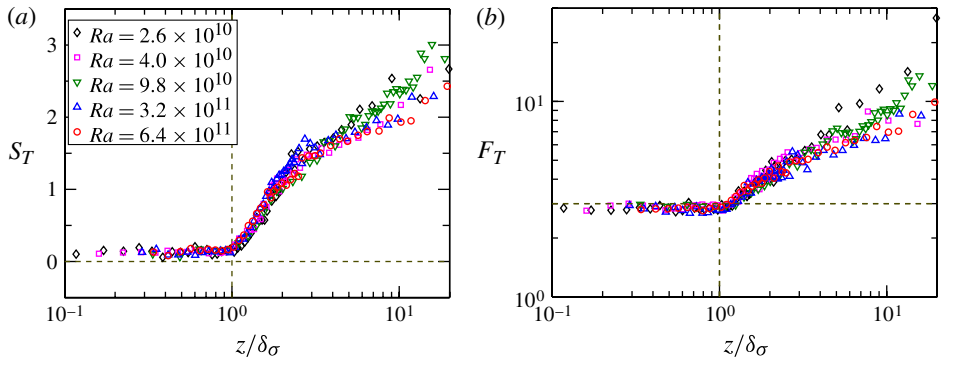

FIGURE 9. (Colour online) Profiles of the skewness S_T (*a*) and the flatness F_T (*b*) of temperature. Here the vertical distance z has been normalized by the thermal BL thickness δ_σ.

little bit skewed toward high temperature values. Second is the central core region in which the turbulent flow is approximately locally homogeneous and isotropic (Zhou, Sun & Xia 2008; Zhou *et al.* 2011*a*) and the temperature distribution is symmetric and has two exponential tails. Hence, S_T is close to zero, while F_T seems to be around the value of six, which is the characteristic value of the flatness for a exponentially distributed quantity. In the intermediate region S_T and F_T first increase at increasing z. After reaching the maximum, both quantities drop towards the cell centre. This hill-like portions of the skewness and flatness profiles signify that the turbulent flow in such region is highly anisotropic. This is due to the presence of hot plumes that ascend from the heating plate. Therefore, this region corresponds to the so-called mixing zone (Castaing *et al.* 1989) and the temperature skewness and flatness profiles in figure 8 can provide a quantitative way to characterize the mixing zone. It is of great interest to note that the mixing zone found here is roughly the same as that determined based on the skewness of 'plus' and 'minus' temperature increments (Zhou & Xia 2002). Note also that the similar changes in S_T and F_T have been observed in recent experimental (He & Tong 2009) and numerical (Emran & Schumacher 2008) studies.

To study the universal properties of high-order moments of temperature, we use the r.m.s. thermal BL thickness δ_σ, instead of the cell height H, to normalize the skewness and flatness profiles. Figure 9 shows five typical profiles of S_T and F_T versus z/δ_σ. Compared with the scaled mean-temperature profiles in figure 5, the skewness and flatness profiles are seen to be somewhat scattered. This is because, being high-order quantities, the skewness and the flatness require longer time average than the mean value for the same level of statistical accuracy. Nevertheless, one sees that over a wide range of Ra and near the thermal BL both S_T and F_T profiles can collapse onto a single curve irrespective of Ra, again suggesting that the 'high-order quantities' are more universal than the mean quantities in turbulent thermal convection. Note that the profiles of the temperature skewness and flatness presented here also reveal some different features when compared with those found in air-filled cells (Maystrenko *et al.* 2007; du Puits *et al.* 2007*b*), where the temperature skewness is found to vanish at $z \approx \delta_{th}$ and there exists a 'dip' region on the flatness profiles in which the temperature flatness drops slightly below $F_T = 3$. These differences could be the large difference in Prandtl number in the two experiments: in air, $Pr = 0.7$, which is approximately six times smaller than that in our system. Another possible reason for this difference is that the high-order temperature profiles in the working fluid of a mixture like air may

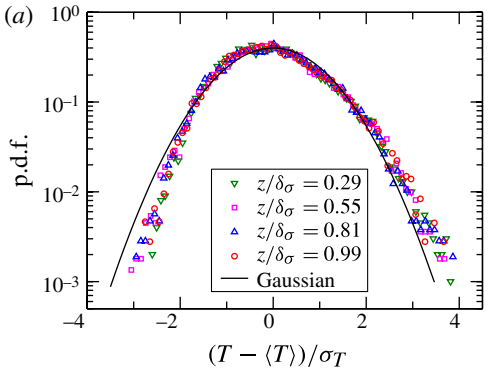

FIGURE 10. (Colour online) P.d.f.s of the scaled temperature $(T - \langle T \rangle)/\sigma_T$ measured at four different vertical distances $z \lesssim \delta_\sigma$ from the bottom plate for $Ra = 3.2 \times 10^{11}$. The black solid curve indicates a Gaussian distribution of variance of one.

exhibit different behaviours from those in a pure working fluid such as water as used in our measurements (Ahlers *et al.* 2009).

3.3. *Self-similar regime within the thermal BL*

The temperature skewness and flatness profiles in figure 9 show that within the range $z \lesssim \delta_\sigma$ both S_T and F_T are nearly invariant irrespective of the measuring position. This feature implies self-similar properties for temperature within such range. To test this, we plot in figure 10 the p.d.f.s of temperature obtained at four different vertical distances $z \lesssim \delta_\sigma$ from the bottom plate for $Ra = 3.2 \times 10^{11}$. Here, the fluctuating temperature $(T - \langle T \rangle)$ has been normalized by its standard deviation σ_T. One sees that after normalization all of these p.d.f.s collapse on top of each other, except a little scatter near the tails which is probably due to the limited statistics. When compared with the Gaussian distribution (the black solid line in figure 10), a small deviation can be observed, i.e. the p.d.f.s are slightly skewed toward right or higher temperature values. This small deviation from the Gaussian distribution would lead to a positive temperature skewness and to a temperature flatness that is slightly smaller than three. Taken together, the p.d.f.s in figure 10 illustrate that near the plate or inside the thermal BL (for $z \lesssim \delta_\sigma$) there exists a self-similar regime, within which the fluctuating temperature obeys an universal distribution that is slightly deviated from the Gaussian one. We further found that this self-similar regime holds for all investigated values of Ra.

3.4. *Properties of the temperature time derivative profiles*

We turn next to the profiles of the temperature time derivative. In the calculation of the derivative we have adopted $dT_i = T_i - T_{i-1}$ using the discrete time series T_i to characterize $\partial T/\partial t$ (Belmonte & Libchaber 1996; Sun & Xia 2007) and hence the r.m.s., skewness and flatness of the temperature derivative can be calculated as

$$\sigma'_T = \langle dT_i^2 \rangle^{1/2}, \tag{3.2a}$$

$$S'_T = \langle dT_i^3 \rangle / \sigma_T'^3, \tag{3.2b}$$

$$F'_T = \langle dT_i^4 \rangle / \sigma_T'^4. \tag{3.2c}$$

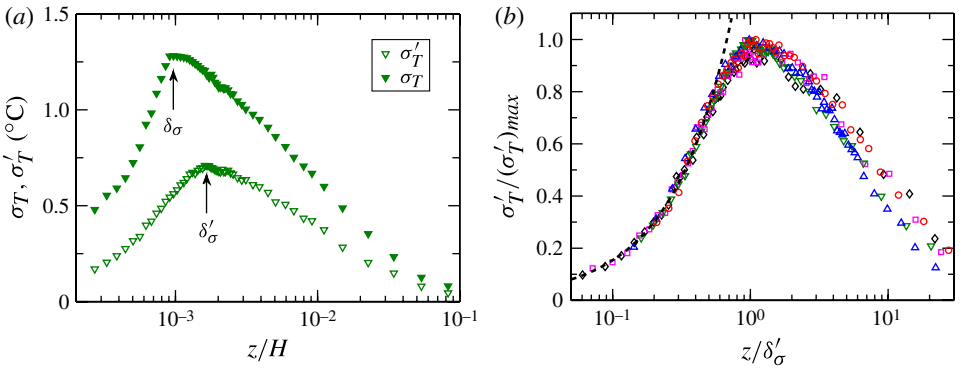

FIGURE 11. (Colour online) (*a*) Profiles of the temperature r.m.s. σ_T and the r.m.s. of the temperature derivative σ'_T for $Ra = 3.2 \times 10^{10}$. (*b*) Profiles of $\sigma'_T/(\sigma'_T)_{max}$ versus the normalized vertical distance z/δ'_σ for $Ra = 2.6 \times 10^{10}$ (circles), 4.0×10^{10} (squares), 9.8×10^{10} (up-triangles), 3.2×10^{11} (down-triangles) and 6.4×10^{11} (diamonds). The dashed line is a linear fit: $\sigma'_T/(\sigma'_T)_{max} = (1.47 \pm 0.03) z/\delta'_\sigma$.

Figure 11(*a*) shows a typical profile of σ'_T versus the normalized distance from the bottom plate z/H in a semi-log plot at $Ra = 3.2 \times 10^{10}$. For comparison, we also plot in the figure the profile of the temperature r.m.s. σ_T measured at the same Ra. It is seen that σ'_T shares the similar shape as σ_T, i.e. σ'_T first increases near the plate and then decreases after reaching its maximum. This feature is consistent with those found in a cubic cell filled with pressurized gas by Belmonte & Libchaber (1996). However, because of the limited spatial resolution, their data could not reveal whether the maximum of σ'_T occurs inside or outside the thermal BL (Belmonte & Libchaber 1996). In the present study, the high-spatial-resolution measurements allow us to examine this more exactly. Here, we define the length scale δ'_σ as the vertical distance from the plate at which the maximum of σ'_T occurs and our results shows that the relationship $\delta'_\sigma > \delta_{th} > \delta_\sigma$ (see table 2) holds for all Ra, suggesting that the maximum of σ'_T occurs outside the thermal BL which may be due to the emissions of plumes from the BLs.

To compare the σ'_T profiles obtained at different Ra, we plot in figure 11(*b*) σ'_T normalized by its maximum value $(\sigma'_T)_{max}$ versus z scaled by δ'_σ in a semi-log plot. One sees that for the range $z/\delta'_\sigma < 0.5$ the profiles are independent of Ra and can be well described by a linear relation between σ'_T and z (see the dashed line in figure 11*b*). We further note that the range $z/\delta'_\sigma < 0.5$ is roughly the same as the self-similar regime of the thermal BL as discussed in § 3.3. For $z/\delta'_\sigma > 1$ the profiles are found to vary with Ra, i.e. they cannot be scaled onto a single curve. This is in contrast to the profiles of the temperature r.m.s. σ_T where the shape universality with respect to different Ra holds over the whole range of z investigated, from the BL to the convective central core. This difference might be explained by the increased calculation error due to the evaluation of the time derivatives.

Figure 12(*a*) shows three typical profiles of the skewness of the temperature derivative. Here, the vertical distance has been normalized by the r.m.s. thermal BL thickness δ_σ. It is found that all of these profiles follow a similar shape, i.e. S'_T is positive and keeps nearly constant near the plate and then increases to form a small and somewhat broad peak; and after reaching its maximum $(S'_T)_{max}$ around $z = \delta_\sigma$, it decreases to the value $S'_T < 0$ in the bulk regime. Nevertheless, we find that the S'_T

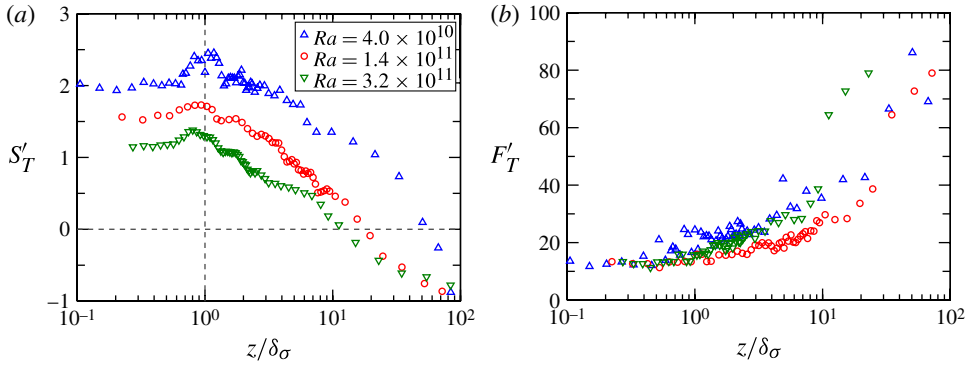

FIGURE 12. (Colour online) Profiles of the skewness S'_T (*a*) and the flatness F'_T (*b*) of the temperature derivative for three different Ra.

No.	Ra	Nu	δ_{th} (mm)	δ_σ (mm)	δ'_σ (mm)
1	2.64×10^{10}	210.0	1.80	1.14	2.17
2	4.00×10^{10}	232.2	1.47	0.97	2.03
3	6.28×10^{10}	254.5	1.21	0.79	1.70
4	9.75×10^{10}	300.4	1.16	0.75	1.26
5	1.38×10^{11}	317.7	1.02	0.68	1.13
6	1.89×10^{11}	346.2	0.98	0.61	1.10
7	2.34×10^{11}	383.7	0.84	0.54	1.12
8	2.85×10^{11}	413.8	0.79	0.53	1.10
9	3.24×10^{11}	433.3	0.72	0.48	0.83
10	4.38×10^{11}	481.0	0.68	0.46	0.72
11	6.41×10^{11}	506.7	0.59	0.41	0.66

TABLE 2. Measured values of Nu, of the thermal BL thickness δ_{th} and δ_σ, and of the length scale δ'_σ at various Ra.

profiles for different Ra cannot be brought to collapse onto each other, in contrast to the universal shape of S_T within the thermal BL. We also note that the magnitude of S'_T near the thermal BL is of order one, the same size as that found by Belmonte & Libchaber (1996), but decreases at increasing Ra. The details about the Ra dependence of S'_T will be discussed in § 3.5.

The flatness profiles of the temperature derivative for three different Ra are plotted in figure 12(*b*). Although the data look somewhat scattered, all of these profiles follow a certain trend. Inside the thermal BL and near the plate, F'_T remains nearly a constant value, which is of the order of 10 and is much larger than the characteristic value of 3 for data with a Gaussian distribution. The large deviation of F'_T from the Gaussian value reflects the well-known property of small-scale persistence of intermittency, which is believed to originate from the sharp fronts of thermal plumes in the present case. When z is increased toward the bulk region, F'_T increases from of the order of 10 near the thermal BL to of the order of 100 in the mixing zone. The increased magnitude of F'_T implies the enhanced small-scale intermittency, which may be due to the mixing, merging and clustering of thermal plumes.

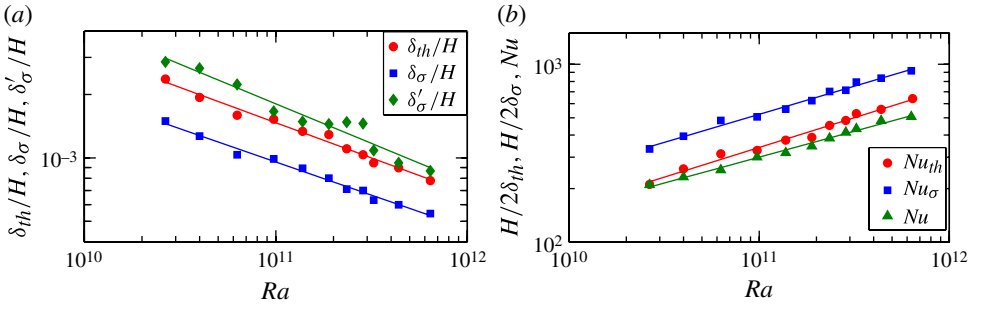

FIGURE 13. (Colour online) (*a*) Normalized thermal BL thicknesses δ_{th}/H and δ_σ/H and normalized length scale δ'_σ/H versus Ra. The three solid lines are power-law fits: $\delta_{th}/H = (6.85 \pm 0.70)Ra^{-0.33\pm0.03}$ (line through the circles, shown in red online), $\delta_\sigma/H = (2.86 \pm 0.30)Ra^{-0.31\pm0.03}$ (line through the squares, shown in blue online) and $\delta'_\sigma/H = (25 \pm 3)Ra^{-0.38\pm0.05}$ (line through the diamonds, shown in green online) to the respective data. (*b*) The pointwise Nusselt number Nu_{th} and Nu_σ determined from the thermal BL thickness using (3.4) and the measured Nu versus Ra. The three solid lines are power-law fits: $Nu_{th} = (0.07 \pm 0.01)Ra^{0.33\pm0.03}$ (line through the circles, shown in red online), $Nu_\sigma = (0.17 \pm 0.02)Ra^{0.31\pm0.03}$ (line through the squares, shown in blue online) and $Nu = (0.19 \pm 0.02)Ra^{0.29\pm0.03}$ (line through the triangles, shown in green online) to the respective data.

3.5. *Ra dependence of the thermal BL properties*

In this subsection, we discuss the scaling properties of the thermal BL thickness with the Rayleigh number Ra and compare results based on the two different definitions as discussed in § 1.1. Figure 13(*a*) shows the Ra dependence of the thermal BL thicknesses normalized by the cell height H. The circles represent δ_{th}/H and the squares represent δ_σ/H. Also shown as the diamonds in the figure is the normalized length scale δ'_σ/H. The three solid lines represent the best power-law fits to the corresponding data and give

$$\delta_{th}/H = (6.85 \pm 0.70)Ra^{-0.33\pm0.03}, \tag{3.3a}$$

$$\delta_\sigma/H = (2.86 \pm 0.30)Ra^{-0.31\pm0.03}, \tag{3.3b}$$

$$\delta'_\sigma/H = (25 \pm 3)Ra^{-0.38\pm0.05}. \tag{3.3c}$$

It is seen that within experimental uncertainties the two BL thicknesses δ_{th} and δ_σ defined differently have essentially the same scaling behaviour with respect to Ra but their magnitudes differ by roughly a factor of two, with δ_{th} being the larger. While the length scale δ'_σ exhibits a little steeper decaying exponent. The present Ra-scaling exponent of -0.33 ± 0.03 of the thermal BL thickness is in excellent agreement with our previous measurements in a rectangular cell over a relatively lower Ra range (Sun *et al.* 2008) and is comparable with the results of earlier experiments performed in cubic cells (Belmonte *et al.* 1993, 1994; Lui & Xia 1998) and in cylindrical cells (Wang & Xia 2003) (see table 1) and is also consistent with some numerical studies (Verzicco & Camussi 2003; Verzicco & Sreenivasan 2008; Wagner, Shishkina & Wagner 2012).

With the measured thermal BL thickness, one can define the pointwise Nusselt numbers Nu_{th} and Nu_σ as (Belmonte *et al.* 1994)

$$Nu_{th} = \frac{H}{2\delta_{th}} \quad \text{and} \quad Nu_\sigma = \frac{H}{2\delta_\sigma}. \tag{3.4}$$

As the thermal BL thickness would impose on and limit the amount of the global heat transport across the cell, the total heat flux of the system may be expected to have the same Ra dependence as that of the thermal BL thickness. It has been shown by early experiments in gas (Belmonte *et al.* 1994) that Nu_{th} measured at the centre of the top plate can indeed characterize the total heat flux Nu, i.e. Nu_{th} has the same scaling exponent with Ra and approximately the same magnitude as Nu. However, later measurements in water (Lui & Xia 1998) suggested that the thermal BL thickness measured at the centre of the plate is not sufficient to characterize the global heat flux in a quantitative way and hence pointed out that caution must be taken when generalizing the obtained results to the whole cell from the measured scaling properties for local quantities.

Figure 13(*b*) shows the Ra dependence of Nu_{th} and Nu_σ converted, respectively, from the measured δ_{th} and δ_σ using (3.4). Also shown in the figure is the global heat flux Nu obtained by assuming a negligible heat leakage through the sidewalls and the bottom plate of the convection cell. The three solid lines in the figure represent the best power-law fits to the corresponding data and give

$$Nu_{th} = (0.07 \pm 0.01)Ra^{0.33\pm0.03}, \tag{3.5a}$$

$$Nu_\sigma = (0.17 \pm 0.02)Ra^{0.31\pm0.03}, \tag{3.5b}$$

$$Nu = (0.19 \pm 0.02)Ra^{0.29\pm0.03}. \tag{3.5c}$$

It is seen that within experimental uncertainty Nu_{th}, Nu_σ and Nu have similar scaling behaviours with Ra but their magnitudes differ from each other, with Nu_{th} and Nu_σ being larger than Nu. These features agree well with those found in a water-filled cylindrical cell (Lui & Xia 1998) and imply that the distribution of the thermal BL thickness is not uniform over the plate, such as a 'V'-shaped layer found in cylindrical cell (Lui & Xia 1998), and the system has a thinner layer at the centre of the plate. Note also that Nu_{th} is much closer to the measured Nu than Nu_σ. This is because the global heat transport is limited by thermal conductivity of the BL which is determined by the slope of the mean temperature at the top and bottom plates, rather than by thermal fluctuations.

We next examine the Ra dependence of $(\sigma_T)_{max}$ for the temperature r.m.s. profiles and of $(\sigma_T')_{max}$ for the r.m.s. profiles of the temperature derivative measured along the central axis of the cell. Figure 14(*a*) shows $(\sigma_T)_{max}$ normalized by the temperature difference Δ versus Ra. The solid line in the figure represents the best power-law fit to the data and gives

$$(\sigma_T)_{max}/\Delta = (3.7 \pm 0.4)Ra^{-0.15\pm0.02}. \tag{3.6}$$

Note that the scaling exponent of $(\sigma_T)_{max}/\Delta$ with Ra obtained here is in a good agreement with that found by Wang & Xia (2003) in a cubic cell, but is approximately half the size of that found by Shang, Tong & Xia (2008) at a fixed measuring point near the bottom plate of a cylindrical cell. It is also of great interest to note that our present exponent is the same as that of the fluctuating temperature r.m.s. measured at the cell centre (Castaing *et al.* 1989; Sun & Xia 2007), but is a little smaller than the theoretical value predicted for the plume-dominated region (such as the region near the

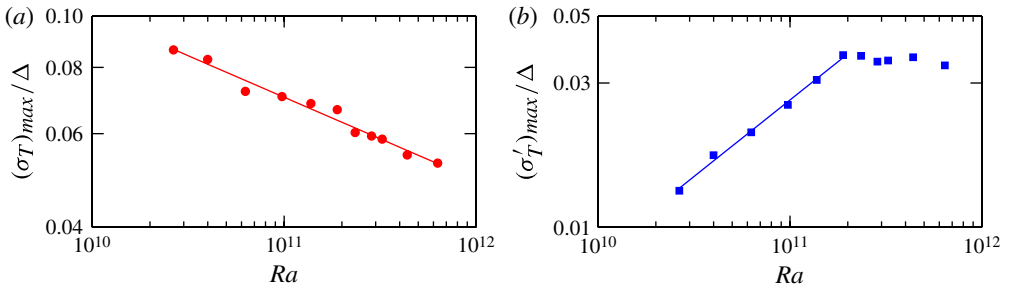

FIGURE 14. (Colour online) Normalized maximum value $(\sigma_T)_{max}/\Delta$ of the temperature r.m.s. profile (*a*) and $(\sigma'_T)_{max}/\Delta$ of the r.m.s. profile of the temperature derivative (*b*) versus *Ra*. The solid lines are power-law fits: $(\sigma_T)_{max}/\Delta = (3.7 \pm 0.4)Ra^{-0.15\pm0.02}$ (*a*) and $(\sigma'_T)_{max}/\Delta = (7.2 \pm 0.7) \times 10^{-8}Ra^{0.51\pm0.02}$ (*b*).

plate) and based on the recent scenario of the GL theory (Grossmann & Lohse 2004), where the scaling exponent of the plume-induced thermal fluctuations is found to vary between -0.11 and -0.09 for all given *Pr*.

The maximum of the normalized r.m.s. of the temperature derivative $(\sigma'_T)_{max}/\Delta$ is shown as a function of *Ra* in figure 14(*b*). It is seen that the $(\sigma'_T)_{max}/\Delta$ versus *Ra* relationship has a transition at $Ra \simeq 2 \times 10^{11}$. When *Ra* is below this transition point, $(\sigma'_T)_{max}/\Delta$ increases as *Ra* increases and the relation between the two quantities can be well described by a power function,

$$(\sigma'_T)_{max}/\Delta = (7.2 \pm 0.7) \times 10^{-8}Ra^{0.51\pm0.02}, \tag{3.7}$$

whereas $(\sigma'_T)_{max}/\Delta$ may be regarded as constant within experimental uncertainties when *Ra* is above this transition point.

Note that the ratio between σ_T and $\langle(\partial T/\partial t)^2\rangle^{1/2}$ is a sort of thermal Taylor microtime (Tennekes & Lumley 1972), which can be used to characterize the dynamics of the temperature fluctuations and studied via the dimensionless quantity *Q*,

$$Q = \frac{H^2}{\kappa}\frac{\langle(\partial T/\partial t)^2\rangle^{1/2}}{\sigma_T} \sim \frac{(\sigma'_T)_{max}}{(\sigma_T)_{max}}. \tag{3.8}$$

With the fitting (3.6) and (3.7), we have

$$Q \sim \begin{cases} Ra^{0.66\pm0.04} & \text{for } Ra < 2 \times 10^{11}, \\ Ra^{0.15\pm0.02} & \text{for } Ra > 2 \times 10^{11}. \end{cases} \tag{3.9}$$

For $Ra < 2 \times 10^{11}$, our measured scaling exponent of *Q* versus *Ra* is in excellent agreement with the value 0.68 ± 0.03 obtained by Belmonte & Libchaber (1996) and is comparable with the result of 0.60 ± 0.06 found by Procaccia *et al.* (1991), while for $Ra > 2 \times 10^{11}$, the exponent is much smaller than the value 0.47 ± 0.07 measured in low-temperature helium gas (Procaccia *et al.* 1991). A similar transition for the relation between *Q* and *Ra* has also been observed by Procaccia *et al.* (1991). These authors argued that the transition is due to the decrease of a sort of inner scale, above which thermal plumes would exhibit some fractal properties. However, Grossmann & Lohse (1993) have argued that these changes are due to the limited thermal response

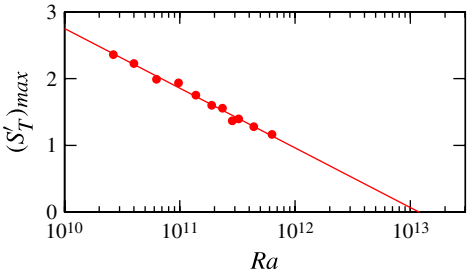

FIGURE 15. (Colour online) The Ra dependence of the maximum skewness $(S'_T)_{max}$ of the temperature derivative in a semi-log plot. The solid line is a logarithmic fit: $(S'_T)_{max} = (-0.89 \pm 0.05)\log_{10}Ra + (11.7 \pm 1.0)$. The extrapolation of experimental data suggests that there exists a certain transition at $Ra \sim 10^{13}$.

time of the probe BL fluid. For the present case, we note that the sampling frequency may have an impact on the transitions of $(\sigma'_T)_{max}$ and Q, as 15 Hz may not be sufficient to resolve properly the time-derivative properties, especially for the high-Ra data. Indeed, Zhou & Xia (2001) has found that the cut-off frequency of temperature is higher than 20 Hz for $Ra = 1.3 \times 10^{11}$.

We finally examine the relation between S'_T and Ra. It has been shown in figure 12(a) that inside the thermal BL S'_T is positive and decreases as Ra is increased. This relation can be well illustrated in figure 15, where the maximum skewness $(S'_T)_{max}$ for the temperature derivative profiles is plotted as a function of Ra in a semi-log scale. It is seen that $(S'_T)_{max}$ drops at increasing Ra and the relation can be described well by a logarithmic function:

$$(S'_T)_{max} = (-0.89 \pm 0.05)\log_{10}Ra(11.7 \pm 1.0). \tag{3.10}$$

It should be noted that the extrapolation of the fitting line crosses $S'_T = 0$ at $Ra \sim 10^{13}$. This suggests that there exists a certain transition for turbulent RB convection. We further note that this critical Ra is consistent with that found by Sun *et al.* (2008), who adopted two independent criterions to show that a BL transition from being laminar to being turbulent is expected to occur at $Ra \simeq 2 \times 10^{13}$.

4. Summary and conclusion

In conclusion, we have made a systematic study of the thermal BL properties in a water-filled rectangular cell by performing high-spatial-resolution measurements of temperature near the bottom plate, along the vertical axis that passes through the centre of the plate, with the Prandtl number Pr fixed at 4.3 and the Rayleigh number varying from 2×10^{10} to 7×10^{11}. The system of the turbulent RB convection can be divided into several regimes, such as the BLs, the mixing zone and the region of convective central core (Castaing *et al.* 1989). Among these regimes, the BLs, in spite of the small volume fraction they occupy, play a crucial role in the determination of the dynamics of the system, especially the turbulent heat transfer and temperature and velocity statistics. In the present study, from the measured temperature and temperature derivative profiles, we obtain the following physical picture about the thermal BL properties in turbulent RB convection.

First, the distance δ_σ from the plate to the maximal temperature r.m.s. position is a natural length scale for characterizing the statistical properties of thermal BL

quantities, as the r.m.s., skewness and flatness of the temperature field are all sharply different below and above this length scale, i.e. below δ_σ, σ_T increases linearly with the vertical distance z from the plate and S_T is close to zero and F_T is close to three and both quantities remains nearly constant, whereas above δ_σ the decay of σ_T obeys a logarithmic behaviour and S_T and F_T both exhibit a hill-like structure.

Second, there is a self-similar regime near the plate and inside the thermal BL ($z \lesssim \delta_\sigma$). Within the regime, the mean temperature $\langle T \rangle$, the fluctuating temperature r.m.s. σ_T and the r.m.s. of the temperature derivative σ_T' all obey a linear dependence on the vertical distance z from the plate. In addition, the temperature fluctuations, due to the influence of hot plumes, are skewed a little towards higher temperature values and follow a universal distribution, which differs slightly from the Gaussian distribution. This universal distribution can be manifested by constant values of the high-order moments of temperature, such as the skewness and flatness studied in § 3.2.

Third, most profiles studied in the present work, when properly scaled, are found to exhibit certain invariance with respect to *Ra* or show similar features within and near the thermal BL, further signifying the universality of the BLs. Moreover, it is observed that the profiles of the second moment of temperature possess a higher level of universality in comparison with the mean temperature profiles. For the third and fourth moments, scatter due to limited data statistics makes this trend less certain. If this observation can be confirmed in future studies, it then suggests that the 'high-order quantities' are more universal than the mean quantities in turbulent thermal convection.

Finally, the extrapolation of the measured derivative skewness suggests that there exists a certain transition at $Ra \sim 10^{13}$.

Acknowledgements

This work was supported in part by the Natural Science Foundation of China (NSFC) under grant numbers 11222222, 11161160554 and 11002085 and Innovation Program of Shanghai Municipal Education Commission under grant number 13YZ008 (Q.Z.) and in part by Research Grants Council (RGC) of Hong Kong SAR under project number CUHK404409 and the NSFC/RGC Joint Research Scheme under grant number N_CUHK462/11 (K.-Q.X.).

REFERENCES

ADRIAN, R. J. 1996 Variation of temperature and velocity fluctuations in turbulent thermal convection over horizontal surfaces. *Intl J. Heat Mass Transfer* **39**, 2303–2310.

AHLERS, G., BODENSCHATZ, E., FUNFSCHILLING, D., GROSSMANN, S., HE, X.-Z., LOHSE, D., STEVENS, R. J. A. M. & VERZICCO, R. 2012 Logarithmic temperature profiles in turbulent Rayleigh–Bénard convection. *Phys. Rev. Lett.* **109**, 114501.

AHLERS, G., GROSSMANN, S. & LOHSE, D. 2009 Heat transfer and large scale dynamics in turbulent Rayleigh–Bénard convection. *Rev. Mod. Phys.* **81**, 503–537.

AHLERS, G. & XU, X.-C. 2001 Prandtl-number dependence of heat transport in turbulent Rayleigh–Bénard convection. *Phys. Rev. Lett.* **86**, 3320–3323.

ASHKENAZI, S. & STEINBERG, V. 1999 High Rayleigh number turbulent convection in a gas near the gas–liquid critical point. *Phys. Rev. Lett.* **83**, 3641–3644.

BELMONTE, A. & LIBCHABER, A. 1996 Thermal signature of plumes in turbulent convection: the skewness of the derivative. *Phys. Rev.* E **53**, 4893–4898.

BELMONTE, A., TILGNER, A. & LIBCHABER, A. 1993 Boundary layer length scales in thermal turbulence. *Phys. Rev. Lett.* **70**, 4067–4070.

BELMONTE, A., TILGNER, A. & LIBCHABER, A. 1994 Temperature and velocity boundary layers in turbulent convection. *Phys. Rev.* E **50**, 269–279.

BROWN, E. & AHLERS, G. 2006 Rotations and cessations of the large-scale circulation in turbulent Rayleigh–Bénard convection. *J. Fluid Mech.* **568**, 351–386.

CASTAING, B., GUNARATNE, G., HESLOT, F., KADANOFF, L., LIBCHABER, A., THOMAE, S., WU, X.-Z., ZALESKI, S. & ZANETTI, G. 1989 Scaling of hard thermal turbulence in Rayleigh–Bénard convection. *J. Fluid Mech.* **204**, 1–30.

CHAVANNE, X., CHILLA, F., CASTAING, B., HEBRAL, B., CHABAUD, B. & CHAUSSY, J. 1997 Observation of the ultimate regime in Rayleigh–Bénard convection. *Phys. Rev. Lett.* **79**, 3648–3651.

CHAVANNE, X., CHILLÀ, F., CHABAUD, B., CASTAING, B. & HÉBRAL, B. 2001 Turbulent Rayleigh–Bénard convection in gaseous and liquid He. *Phys. Fluids* **13**, 1300–1320.

CHILLÁ, F., CILIBERTO, S., INNOCENTI, C. & PAMPALONI, E. 1993 Boundary layer and scaling properties in turbulent thermal convection. *Il Nuovo Cimento* D **15**, 1229–1249.

CHILLÀ, F. & SCHUMACHER, J. 2012 New perspectives in turbulent Rayleigh–Bénard convection. *Eur. Phys. J.* E **35**, 58.

CHING, E. S. C. 1997 Heat flux and shear rate in turbulent convection. *Phys. Rev.* E **55**, 1189–1192.

DUBRULLE, B. 2001 Logarithmic corrections to scaling in turbulent thermal convection. *Eur. Phys. J.* B **21**, 295–304.

DUBRULLE, B. 2002 Scaling in large Prandtl number burbulent thermal convection. *Eur. Phys. J.* B **28**, 361.

EMRAN, M. S. & SCHUMACHER, J. 2008 Fine-scale statistics of temperature and its derivatives in convective turbulence. *J. Fluid Mech.* **611**, 13–34.

FERNANDES, R. L. J. & ADRIAN, R. J. 2002 Scaling of velocity and temperature fluctuations in turbulent thermal convection. *Exp. Therm. Fluid Sci.* **26**, 355–360.

FUNFSCHILLING, D., BROWN, E., NIKOLAENKO, A. & AHLERS, G. 2005 Heat transport by turbulent Rayleigh–Bénard convection in cylindrical samples with aspect ratio one and larger. *J. Fluid Mech.* **536**, 145–154.

GLAZIER, J. A., SEGAWA, T., NAERT, A. & SANO, M. 1999 Evidence against ultrahard thermal turbulence at very high Rayleigh numbers. *Nature* **398**, 307–310.

GROSSMANN, S. & LOHSE, D. 1993 Characteristic scale in Rayleigh–Bénard-convection. *Phys. Rev.* A **173**, 58–62.

GROSSMANN, S. & LOHSE, D. 2000 Scaling in thermal convection: a unifying theory. *J. Fluid Mech.* **407**, 27–56.

GROSSMANN, S. & LOHSE, D. 2001 Thermal convection for large Prandtl numbers. *Phys. Rev. Lett.* **86**, 3316–3319.

GROSSMANN, S. & LOHSE, D. 2004 Fluctuations in turbulent Rayleigh–Bénard convection: the role of plumes. *Phys. Fluids* **16**, 4462–4472.

GROSSMANN, S. & LOHSE, D. 2011 Multiple scaling in the ultimate regime of thermal convection. *Phys. Fluids* **23**, 045108.

HE, X.-Z., FUNFSCHILLING, D., NOBACH, H., BODENSCHATZ, E. & AHLERS, G. 2012 Transition to the ultimate regime in Rayleigh–Bénard convection. *Phys. Rev. Lett.* **108**, 024502.

HE, X.-Z. & TONG, P. 2009 Measurements of the thermal dissipation field in turbulent Rayleigh–Bénard convection. *Phys. Rev.* E **79**, 026306.

LAM, S., SHANG, X.-D., ZHOU, S.-Q. & XIA, K.-Q. 2002 Prandtl number dependence of the viscous boundary layer and the Reynolds numbers in Rayleigh–Bénard convection. *Phys. Rev.* E **65**, 066306.

LI, L., SHI, N., DU PUITS, R., RESAGK, C., SCHUMACHER, J. & THESS, A. 2012 Boundary layer analysis in turbulent Rayleigh–Bénard convection in air: experiment versus simulation. *Phys. Rev.* E **86**, 026315.

LOHSE, D. & XIA, K.-Q. 2010 Small-scale properties of turbulent Rayleigh–Bénard convection. *Annu. Rev. Fluid Mech.* **42**, 335–364.

LUI, S.-L. & XIA, K.-Q. 1998 Spatial structure of the thermal boundary layer in turbulent convection. *Phys. Rev.* E **57**, 5494–5503.

MALKUS, M. V. R. 1951 The heat transport and spectrum of thermal turbulence. *Proc. R. Soc. Lond.* A **225**, 196–212.

MAYSTRENKO, A., RESAGK, C. & THESS, A. 2007 Structure of the thermal boundary layer for turbulent Rayleigh–Bénard convection of air in a long rectangular enclosure. *Phys. Rev.* E **75**, 066303.

NAERT, A., SEGAWA, T. & SANO, M. 1997 High-Reynolds-number thermal turbulence in mercury. *Phys. Rev.* E **56**, R1302.

NIEMELA, J. J., SKRBEK, L., SREENIVASAN, K. R. & DONNELLY, R. J. 2000 Turbulent convection at very high Rayleigh numbers. *Nature* **404**, 837–840.

NIEMELA, J. J. & SREENIVASAN, K. R. 2003 Rayleigh-number evolution of large-scale coherent motion in turbulent convection. *Europhys. Lett.* **62**, 829.

NIEMELA, J. J. & SREENIVASAN, K. R. 2006 Turbulent convection at high Rayleigh numbers and aspect ratio 4. *J. Fluid Mech.* **557**, 411–422.

POHLHAUSEN, E. 1921 Wärmetausch zwischen festen Körpern und Flüssigkeiten mit kleiner Reibund und kleiner Wärmeleitung. *Z. Angew. Math. Mech.* **1**, 115.

PRANDTL, L. 1932 Meteorologische anwendungen der stroemungslehre. *Beitr. Phys. Atmos.* **19**, 188–202.

PRIESTLEY, C. H. B. 1959 *Turbulent Transfer in the Lower Atmosphere*. University of Chicago Press.

PROCACCIA, I., CHING, E. S. C., CONSTANTIN, P., KADANOFF, L. P., LIBCHABER, A. & XU, X.-Z. 1991 Transitions in convective turbulence: the role of thermal plumes. *Phys. Rev.* A **44**, 8091–8102.

DU PUITS, R., RESAGK, C. & THESS, A. 2007*a* Mean velocity profile in confined turbulent convection. *Phys. Rev. Lett.* **99**, 234504.

DU PUITS, R., RESAGK, C., TILGNER, A., BUSSE, F. H. & THESS, A. 2007*b* Structure of the thermal boundary layer in turbulent Rayleigh–Bénard convection. *J. Fluid Mech.* **572**, 231–254.

ROCHE, P.-E., CASTAING, B., CHABAUD, B. & HÉBRAL, B. 2002 Prandtl and Rayleigh numbers dependences in Rayleigh–Bénard convection. *Europhys. Lett.* **58**, 693.

ROCHE, P.-E., GAUTHIER, F., KAISER, R. & SALORT, J. 2010 On the triggering of the ultimate regime of convection. *New J. Phys.* **12**, 085014.

SCHEEL, J. D., KIM, E. & WHITE, K. R. 2012 Thermal and viscous boundary layers in turbulent Rayleigh–Bénard convection. *J. Fluid Mech.* **711**, 281–305.

SHANG, X.-D., TONG, P. & XIA, K.-Q. 2008 Scaling of the local convective heat flux in turbulent Rayleigh–Bénard convection. *Phys. Rev. Lett.* **100**, 244503.

SHI, N., EMRAN, M. S. & SCHUMACHER, J. 2012 Boundary layer structure in turbulent Rayleigh–Bénard convection. *J. Fluid Mech.* **706**, 5–33.

SHISHKINA, O. & THESS, A. 2009 Mean temperature profiles in turbulent Rayleigh–Bénard convection of water. *J. Fluid Mech.* **633**, 449–460.

SHRAIMAN, B. I. & SIGGIA, E. D. 1990 Heat transport in high-Rayleigh-number convection. *Phys. Rev.* A **42**, 3650.

STEVENS, R. J. A. M., ZHOU, Q., GROSSMANN, S., VERZICCO, R., XIA, K.-Q. & LOHSE, D. 2012 Thermal boundary layer profiles in turbulent Rayleigh–Bénard convection in a cylindrical sample. *Phys. Rev.* E **85**, 027301.

SUN, C., CHEUNG, Y.-H. & XIA, K.-Q. 2008 Experimental studies of the viscous boundary layer properties in turbulent Rayleigh–Bénard convection. *J. Fluid Mech.* **605**, 79–113.

SUN, C., REN, L.-Y., SONG, H. & XIA, K.-Q. 2005 Heat transport by turbulent Rayleigh–Bénard convection in 1 m diameter cylindrical cells of widely varying aspect ratio. *J. Fluid Mech.* **542**, 165–174.

SUN, C. & XIA, K.-Q. 2005 Scaling of the Reynolds number in turbulent thermal convection. *Phys. Rev.* E **72**, 067302.

SUN, C. & XIA, K.-Q. 2007 Multi-point local temperature measurements inside the conducting plates in turbulent thermal convection. *J. Fluid Mech.* **570**, 479–489.

TENNEKES, H. & LUMLEY, J. L. 1972 *A First Course in Turbulence*. MIT.

TILGNER, A., BELMONTE, A. & LIBCHABER, A. 1993 Temperature and velocity profiles of turbulent convection in water. *Phys. Rev.* E **47**, R2253.

VERZICCO, R. 2012 Boundary layer structure in confined turbulent thermal convection. *J. Fluid Mech.* **706**, 1–4.

VERZICCO, R. & CAMUSSI, R. 2003 Numerical experiments on strongly turbulent thermal convection in a slender cylindrical cell. *J. Fluid Mech.* **477**, 19–49.

VERZICCO, R. & SREENIVASAN, K. R. 2008 A comparison of turbulent thermal convection between conditions of constant temperature and constant heat flux. *J. Fluid Mech.* **595**, 203–219.

WAGNER, S., SHISHKINA, O. & WAGNER, C. 2012 Boundary layers and wind in cylindrical Rayleigh–Bénard cells. *J. Fluid Mech.* **697**, 336–366.

WANG, J. & XIA, K.-Q. 2003 Spatial variations of the mean and statistical quantities in the thermal boundary layers of turbulent convection. *Eur. Phys. J.* B **32**, 127–136.

XI, H.-D., ZHOU, Q. & XIA, K.-Q. 2006 Azimuthal motion of the mean wind in turbulent thermal convection. *Phys. Rev.* E **73**, 056312.

XI, H.-D., ZHOU, S.-Q., ZHOU, Q., CHAN, T.-S. & XIA, K.-Q. 2009 Origin of the temperature oscillation in turbulent thermal convection. *Phys. Rev. Lett.* **102**, 044503.

XIA, K.-Q., LAM, S. & ZHOU, S.-Q. 2002 Heat-flux measurement in high-Prandtl-number turbulent Rayleigh–Bénard convection. *Phys. Rev. Lett.* **88**, 064501.

XIA, K.-Q., SUN, C. & ZHOU, S.-Q. 2003 Particle image velocimetry measurement of the velocity field in turbulent thermal convection. *Phys. Rev.* E **68**, 066303.

ZHOU, Q., LI, C.-M., LU, Z.-M. & LIU, Y.-L. 2011*a* Experimental investigation of longitudinal space–time correlations of the velocity field in turbulent Rayleigh–Bénard convection. *J. Fluid Mech.* **683**, 94–111.

ZHOU, Q., LIU, B.-F., LI, C.-M. & ZHONG, B.-C. 2012 Aspect ratio dependence of heat transport by turbulent Rayleigh–Bénard convection in rectangular cells. *J. Fluid Mech.* **710**, 260–276.

ZHOU, Q., STEVENS, R. J. A. M., SUGIYAMA, K., GROSSMANN, S., LOHSE, D. & XIA, K.-Q. 2010 Prandtl–Blasius temperature and velocity boundary-layer profiles in turbulent Rayleigh–Bénard convection. *J. Fluid Mech.* **664**, 297–312.

ZHOU, Q., SUGIYAMA, K., STEVENS, R. J. A. M., GROSSMANN, S., LOHSE, D. & XIA, K.-Q. 2011*b* Horizontal structures of velocity and temperature boundary layers in two-dimensional numerical turbulent Rayleigh–Bénard convection. *Phys. Fluids* **23**, 125104.

ZHOU, Q., SUN, C. & XIA, K.-Q. 2007*a* Morphological evolution of thermal plumes in turbulent Rayleigh–Bénard convection. *Phys. Rev. Lett.* **98**, 074501.

ZHOU, S.-Q., SUN, C. & XIA, K.-Q. 2007*b* Measured oscillations of the velocity and temperature fields in turbulent Rayleigh–Bénard convection in a rectangular cell. *Phys. Rev.* E **76**, 036301.

ZHOU, Q., SUN, C. & XIA, K.-Q. 2008 Experimental investigation of homogeneity, isotropy and circulation of the velocity field in buoyancy-driven turbulence. *J. Fluid Mech.* **598**, 361–372.

ZHOU, Q., XI, H.-D., ZHOU, S.-Q., SUN, C. & XIA, K.-Q. 2009 Oscillations of the large-scale circulation in turbulent Rayleigh–Bénard convection: the sloshing mode and its relationship with the torsional mode. *J. Fluid Mech.* **630**, 367–390.

ZHOU, Q. & XIA, K.-Q. 2008 Comparative experimental study of local mixing of active and passive scalars in turbulent thermal convection. *Phys. Rev.* E **77**, 056301.

ZHOU, Q. & XIA, K.-Q. 2010 Measured instantaneous viscous boundary layer in turbulent Rayleigh–Bénard convection. *Phys. Rev. Lett.* **104**, 104301.

ZHOU, S.-Q. & XIA, K.-Q. 2001 Scaling properties of the temperature field in convective turbulence. *Phys. Rev. Lett.* **87**, 064501.

ZHOU, S.-Q. & XIA, K.-Q. 2002 Plume statistics in thermal turbulence: mixing of an active scalar. *Phys. Rev. Lett.* **89**, 184502.